Post Irradiation Examination of Fuel and Core Structural Materials Irradiated in FBTR

N.G. Muralidharan[a], C.N. Venkiteswaran[b], V. Karthik[c], V. Anandraj[d], J. Joseph[e], K.V. Kasivswanathan[f], S. Venugopal[g], T. Jayakumar[h], B. Raj[i]

Abstract. Performance assessment of various in-core materials of Fast Breeder Test Reactor (FBTR) at Kalpakkam has been carried out in the hot cell facility of Radiometallurgy Laboratory at IGCAR. FBTR uses a unique, indigenously developed mixed uranium- plutonium carbide (U0.3 Pu0.7)C as the fuel and 20% CW SS316 as the material for clad and wrapper. Performance evaluation of carbide driver fuel subassemblies through post irradiation examination (PIE) at various burn-up levels was instrumental in extending the fuel burn-up safely to 165 $GW{\cdot}d{\cdot}t^{-1}$ from the initial design burn-up limit of 50 $GW{\cdot}d{\cdot}t^{-1}$. Besides the carbide driver fuel assemblies, the irradiation behavior of various other core materials like the control rod (B4C pellets with stainless steel clad) and the Nickel reflectors have also been investigated. FBTR finds application as a test bed for irradiation experiments of 500 MWe Prototype Fast Breeder Reactor (PFBR) fuel and structural materials. Experimental pin with MOX fuel composition of PFBR has been irradiated in FBTR and examined in the hot cells for assessing the evolution of fuelclad gap evolution in the beginning-of-life and optimizing the duration of pre-conditioning of the fuel in PFBR. As a part of life extension studies of FBTR, an irradiation experiment was carried out to study the changes in mechanical properties of grid plate material at low dose irradiation. This paper will discuss the results of PIE carried out for performance assessment of the unique FBTR mixed carbide fuel and structural materials, control rod, nickel reflector subassembly and test irradiations of grid plate specimens and MOX fuel.

1. INTRODUCTION

The Fast Breeder Test Reactor at Indira Gandhi Centre for Atomic Research (IGCAR), Kalpakkam has been in operation since 1985 with a unique high plutonium content carbide fuel (U0.3 Pu0.7)C as the driver fuel. The core has been progressively expanded by adding Mark II fuel (U0.45 Pu0.55)C and MOX fuel making the core a hybrid one. Performance evaluation of all the in-core materials had been envisaged during the design of FBTR and a series of α-tight hot cells with inert nitrogen atmosphere ventilation was established in the Radio Metallurgy Laboratory (RML) to carry out the post-irradiation examination (PIE) [1]. The concrete shielded hot cells having 1200 mm thick high density concrete wall are designed to handle radioactivity up to 3.7 × 107 GBq. The hot cells have state-of-art equipment for carrying out a wide spectrum of non-destructive as well as destructive metallurgical examinations. The non-destructive techniques employed include visual examination, dimensional measurements, X-ray and neutron radiographic examinations, eddy current testing, leak testing and gamma scanning. The destructive examinations include metallography, fission gas

[a] Indira Gandhi Centre for Atomic Research, India
[b] Indira Gandhi Centre for Atomic Research, India
[c] Indira Gandhi Centre for Atomic Research, India
[d] Indira Gandhi Centre for Atomic Research, India
[e] Indira Gandhi Centre for Atomic Research, India
[f] Indira Gandhi Centre for Atomic Research, India
[g] Indira Gandhi Centre for Atomic Research, India
[h] Indira Gandhi Centre for Atomic Research, India
[i] Indira Gandhi Centre for Atomic Research, India

extraction and analysis, high temperature tensile tests, micro-hardness, swelling measurements, small specimen test techniques and electron microscopy.

Mixed carbide driver fuel and other core structural materials such as the control rod assembly, nickel reflector assembly etc. discharged from FBTR have been examined in the hot cells. Since FBTR is being used for irradiation testing of advanced fuel and structural materials for the future fast reactors, PIE has an increasing role to play in characterizing their irradiation behaviour and in providing feedback to the designers.

2. PIE OF FBTR MIXED CARBIDE FUEL

2.1. Beginning of life performance assessment of carbide fuel

One of the initial concerns of the designers in limiting the linear heat rating and burnup of the FBTR fuel to 250 $W \cdot cm^{-1}$ and 50 $GW \cdot d \cdot t^{-1}$, was the high swelling rate anticipated for the high plutonium content carbide fuel based on the literature data available for carbide fuels up to 30% plutonium. Hence a series of irradiation tests were done on experimental fuel pins having Mark I & Mark II fuel compositions irradiated to low burn-ups from 1.6–10 $GW \cdot d \cdot t^{-1}$ (16–100 effective full power days (EFPD)). The aim of the experimental irradiation was to study the fuel swelling and cracking behaviour in the beginning-of-life period.

The fuel pins were subjected to radiographic and ceramographic examinations during PIE. The examinations revealed that the swelling and cracking of the carbide fuel occurs within a few days of irradiation thus reducing the fuel-clad gap and enhancing the gap conductance. Swelling rate was found to be lower for Mark II fuel as compared to Mark I fuel. The feedback from PIE gave confidence to optimize the conditioning period at lower linear power and to increase the linear heat rating of the fuel progressively to 400 W/cm.

2.2. PIE of FBTR driver fuel subassemblies

Systematic performance evaluation of fuel and structural materials was carried out at different peak burn-ups of (25, 50, 100 and 155) $GW \cdot d \cdot t^{-1}$ to understand the irradiation behaviour. FBTR fuel burn-up was progressively increased to 165 $GW \cdot d \cdot t^{-1}$ after considering the implications of extending the burn-up at each stage. The salient results of the PIE are presented in this section.

2.2.1. Evaluation of fuel performance

Radiographic examination

X-radiography of fuel pins were done at different burnup levels to obtain data on the increase in fuel stack length, reduction in pellet-to-pellet gap and pellet-to-clad gap and fuel pellet integrity. In general, evaluation of the radiographs of fuel pins after 25 $GW \cdot d \cdot t^{-1}$ and 50 $GW \cdot d \cdot t^{-1}$, revealed presence of pellet- to-pellet gaps and pellet-to-clad gaps at the ends of the fuel column. In the case of fuel pins of 100 $GW \cdot d \cdot t^{-1}$ burn-up, the pellet-to-pellet gaps and pellet-to-clad gaps were not discernible at the centre of the fuel column, while pellet-to-pellet gap was still observed at the end of the fuel column. The radiography of 155 $GW \cdot d \cdot t^{-1}$ fuel pins indicated the closure of pellet-to-pellet gap and pellet-to-clad gap almost throughout the length of the fuel column. Fig. 2.1 shows the X-radiographs of the fuel pin of 155 $GW \cdot d \cdot t^{-1}$ burn-up. Fig. 2.2 shows the trend in the increase in fuel stack length as a function of burn-up, expressed in terms of the percentage of the initial fuel stack length (320 mm).

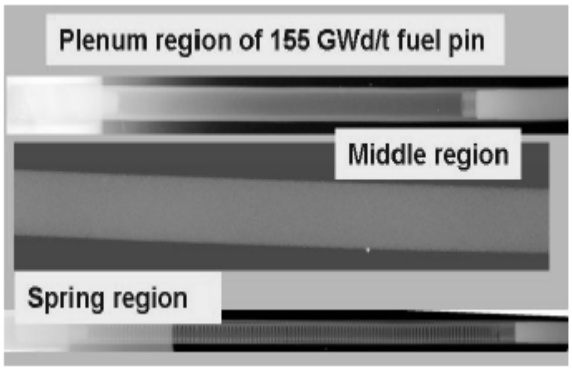

FIG. 2.1. X-radiographs of fuel pins after 155 GW·d·t^{-1} burn-up.

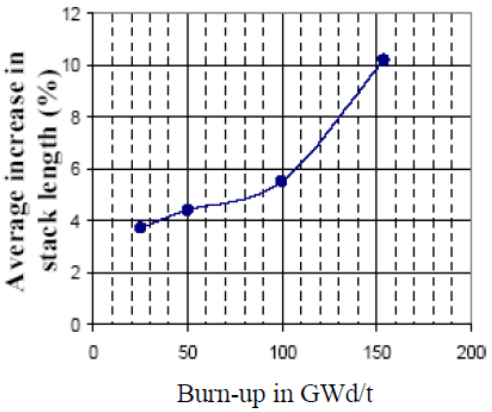

FIG. 2.2. Fuel swelling as a function of burn-up.

Neutron radiography of fuel pins [2] at different burn-ups did not indicate any evidence of actinide redistribution. The fuel stack lengths measured from neutron radiographs compared well with that of the measurements from X- radiographs.

Gamma scanning

Gamma scanning has been carried out on FBTR fuel pins which have seen a peak burnup of 100 GW·d·t^{-1} and 155 GW·d·t^{-1}, to assess the axial fission product distribution. Gamma scanning system inside the hot cell has a precision scanning bench with four axis motorized stages for precise movement of fuel pins with software for automated movement and acquisition of gamma spectrum. Collimators of four different dimensions in the turret assembly established in the hot cell wall facilitate a well-defined region of the fuel pin to be seen by the detector. High purity germanium (HpGe) based gamma spectroscopy system was used for gamma scanning.

Axial distribution profile of different fission products was obtained by acquiring gamma spectrum from various locations along the length of the fuel pin. Gamma scanning clearly revealed migration of caesium from the centre of the fuel column. Plenum regions also indicated the presence of caesium. Axial distribution of ruthenium (Ru106) indicated a smooth profile. Fig 2.3 shows the axial profile of caesium and Ruthenium. Axial flux profile was estimated from the gamma count rates for Ruthenium at various locations of the fuel column and the form factor is around 0.6 which compares well with the reactor physics estimates.

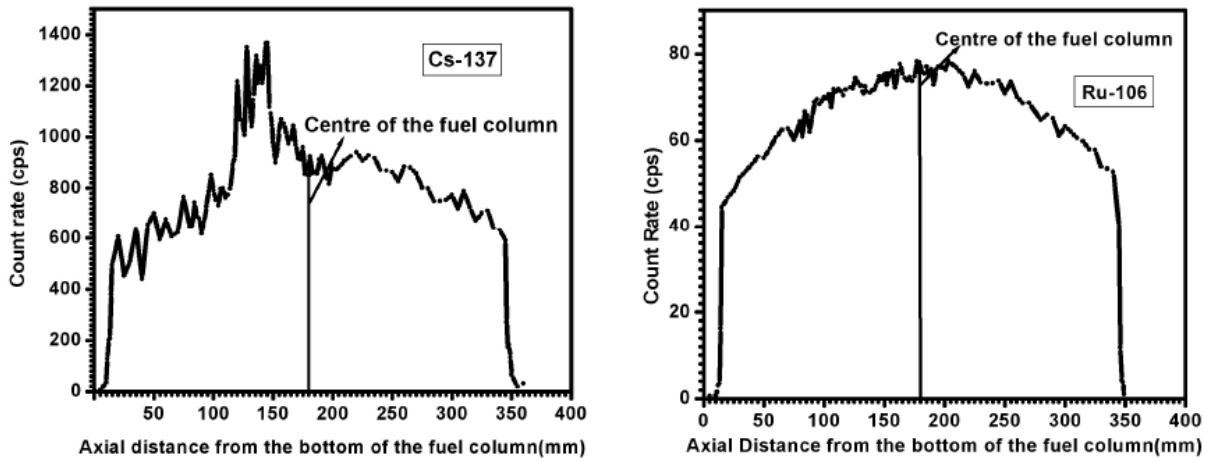

FIG. 2.3. Axial distribution of ruthenium and caesium in the fuel pins.

Fission gas release

Fission gas was extracted by puncturing the fuel pins and the samples were analysed using gas chromatograph. An improved double end fuel pin puncture chamber was used for extraction of fission gas from high burnup fuel pins to facilitate puncturing and collection of fission gas from the top and bottom plenums simultaneously. This was necessitated due to fuel-clad gap closure significantly reducing the communication between the plenum regions.

In 25 GW·d·t^{-1} burn-up fuel pins, fission gas release was found to be less than 1%. In 50 GW·d·t^{-1} burn-up fuel pins, fission gas release varied from 8–18%. Fission gas release measurements after 100 GW·d·t^{-1} burn-up indicated that the gas release is in the range of 4–14% [3]. The lower fission gas release in 100 GW·d·t^{-1} burn-up fuel pins is attributed to the reduction in fuel operating temperatures due to closure of fuel-clad gap. Maximum fission gas release estimated on 155 GW·d·t^{-1} burn-up fuel pins was 16% and the corresponding internal pressure in the fuel pin was measured to be 2.1 MPa. The ratio of xenon to krypton was estimated to be around 13. The helium content in the fuel pins at different burn-ups indicated that most of the helium produced due to alpha decay is released from the fuel matrix to the gas plenum. Fig. 2.4 shows the volume of fission gases released and maximum plenum pressure as a function of burn-up.

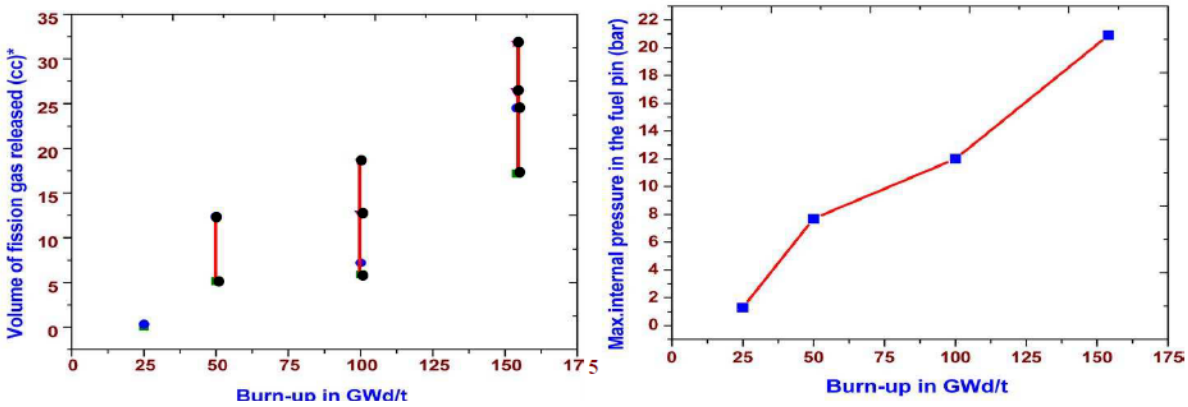

FIG. 2.4. Volume of fission gas released and plenum pressure as a function of burn-up.

Ceramography of fuel-clad cross section

Metallographic examinations of the fuel pin cross sections at various stages of burn-ups has provided valuable information on the fuel-clad gap and microstructural evolution of the carbide fuel. Fig. 2.5 shows the photomosaics of fuel pin cross-sections at the centre of the fuel column after (25, 50, 100 and 155) GW·d·t^{-1} burn-ups. Progressive reduction in the fuel-clad gap and radial cracks were observed in 25 GW·d·t^{-1} and 50 GW·d·t^{-1} burn-up fuel pins. The fuel-clad cross section of 100 GW·d·t^{-1} burn-up fuel pin revealed absence of the gap at the centre of the fuel column with circumferential cracks whereas the cross section at the end of the fuel column indicated presence of fuel-clad gap of a few micrometers with radial cracks.

In 155 GW·d·t^{-1} burn-up fuel pins, the fuel-clad gap had closed completely along the entire length of fuel column with circumferential cracks in the centre and end of the fuel region indicating initiation of fuel clad mechanical interaction (FCMI). The steep increase in the axial stack length of the fuel column beyond 100 GW·d·t^{-1} burn-up measured from X-radiographs (Fig. 2.2) is also indicative of the restrained swelling in the radial direction. Exhaustion of porosities was noticed in the outer rim in 155 burn-up fuel pin at the centre of the fuel column indicating that the fuel is undergoing hot pressing/creep deformation due to fuel swelling under clad restraint. From the pellet diameters

measured by image analysis of photomosaics, the volumetric free swelling rate of fuel was estimated to be around 1.2 at.% burn-up at 25 GW·d·t^{-1} and 1 at.% burn-up at 50 GW·d·t^{-1} [4].

Microstructural examination of the clad did not indicate any evidence of carburization on the inner diameter of the clad tube. Microhardness measurements across the clad wall thickness also did not indicate any significant change in hardness values. Clad inner and outer diameters were measured from the ceramographs. The maximum increase in cross-sectional area was estimated to be around 6.9% which is in good agreement with swelling measurements carried out on the clad.

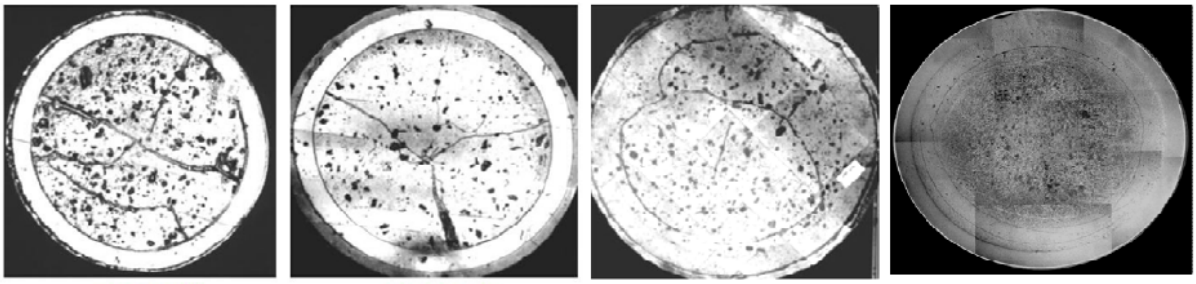

FIG. 2.5. Micrographs of fuel pin cross-sections at the centre of fuel column at various burn-up.

2.2.2. Performance assessment of structural materials

Neutron irradiation of core structural materials induces two types of phenomena (i) changes in dimensions associated with swelling and irradiation creep and (ii) degradation of mechanical properties and embrittlement associated with microstructural evolution [5]. The irradiation induced changes in mechanical properties is a function of neutron fluence (dpa) and the irradiation temperature. The typical axial profile of dpa and irradiation temperature along the core length of the fuel pins in FBTR for 155 GW·d·t^{-1} burn-up fuel subassembly is shown in Fig. 2.6.

Metrology of hexagonal wrapper and cladding

The maximum increase in the dimensions of hexagonal wrapper and fuel pin was seen to occur in the region of peak dpa close to the centre of the fuel column. The trends in the changes in corner-to-corner distance (CCD) and flat-flat distance (FFD) of the wrapper and diametral strain of the fuel pin with dpa are shown in Fig. 2.7. The hexagonal wrapper and the fuel pin did not indicate any increase in their dimensions at low dpa irradiation corresponding to 25 GW·d·t^{-1} and 50 GW·d·t^{-1} burn-ups. Beyond about 30 dpa, the dimensions of both the wrapper and fuel pin were seen to progressively increase with increasing dpa. The rate of increase in the dimensions was higher beyond 100 GW·d·t^{-1} burn-up as compared to that at lower burn-ups. The maximum percentage increase in the fuel pin dimensions was significantly higher than that of hexagonal wrapper dimensions on account of the higher temperatures of the cladding (Fig. 2.6) close to the peak swelling temperatures of 20% cold worked SS316. Similar trends were also observed in the void swelling estimates of clad and wrapper samples determined from density measurements (Fig. 2.7).

Considering a nominal gap of 0.7 mm between adjacent fuel subassemblies in the FBTR core, the dilation of 0.65 mm of the 155 GW·d·t^{-1} burn-up wrapper is one of the factors of concern, from fuel handling considerations, for further increasing the residence time of the fuel subassemblies.

Mechanical properties of cladding and wrapper

The mechanical properties of irradiated SS316 cladding were determined by remote tensile tests carried out on tube specimens sectioned from various locations along the length of the fuel pins corresponding to a combination of dpa (0–83) and irradiation temperature (430–500°C). The tests

were conducted at temperatures corresponding to (i) reactor operation conditions (ii) fuel handling operations (180ºC) and (ii) ambient conditions (25ºC). It was seen that the ultimate tensile strength (UTS) of the cladding shows a significant decrease at displacement damages >60 dpa both in high temperature and room temperature tests, while the uniform elongation was around 3–4.5% (Fig. 8). Similar trends of decreasing UTS with increasing dpa have been reported in the literature [6].

The tensile properties of the hexagonal wrapper were evaluated by shear punch tests involving blanking a 1.0 mm thick and 8.0 mm diameter specimen in a test fixture using a flat cylindrical punch. The load-displacement plot obtained during the punching operation was analyzed and correlated with the conventional tensile test data. Tensile-to-shear punch property correlation was established from standardization experiments on various cold rolled and solution annealed specimens of SS316. Shear punch tests were carried out at room temperature and irradiation temperature on the specimens extracted from wrapper. The results indicate that there is an increase in the yield strength (YS) and the UTS with increasing dpa (Figs 2.9–2.10) and a decrease in the ductility. The tensile properties of the wrapper showed a hardening behaviour as its irradiation temperature is around 400–430ºC.

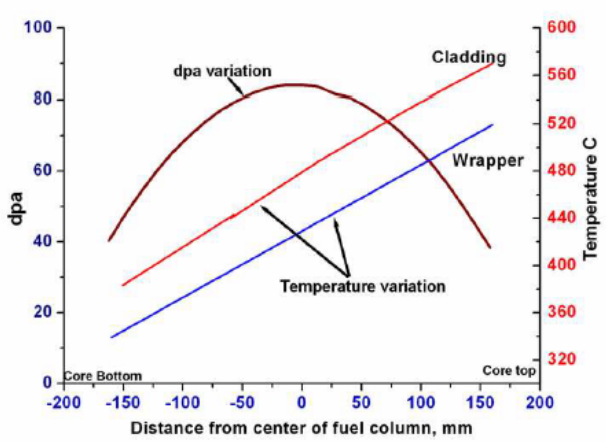

FIG. 2.6. Typical axial profile of dpa and irradiation temperature along the core for the 155GWd/t burnup fuel subassembly.

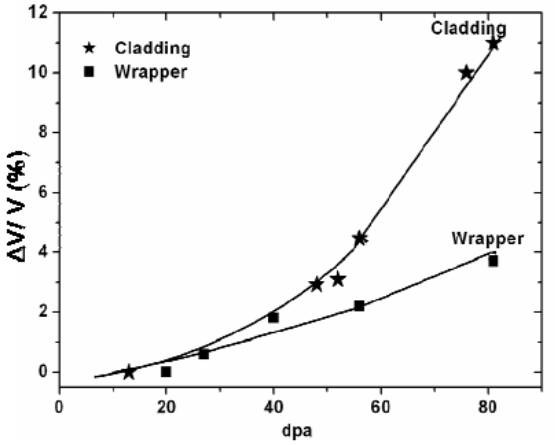

FIG. 2.7. Trends in void swelling of FBTR clad and wrapper with dpa from density measurements.

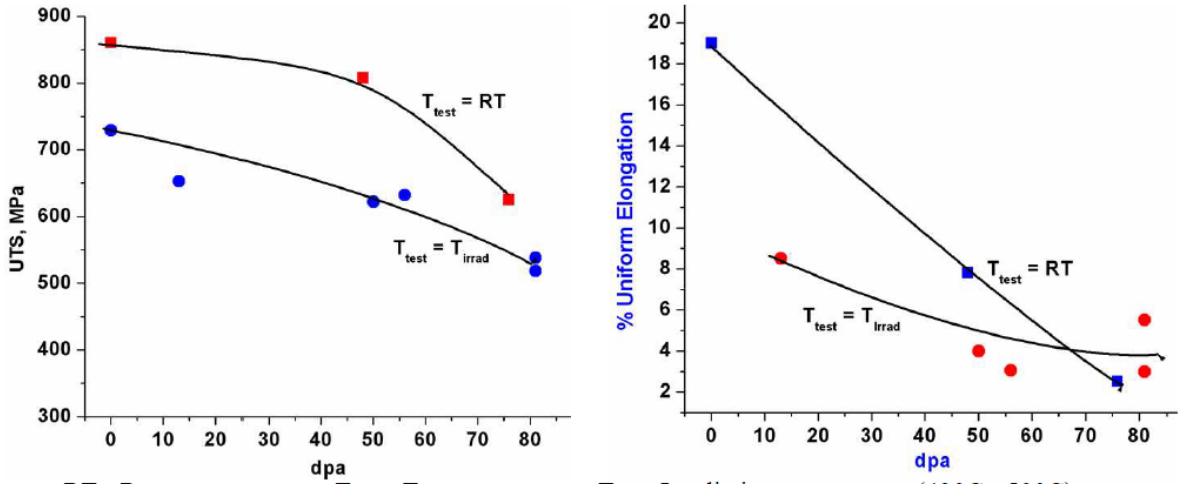

RT - Room temperature, T_{test} – Test temperature, T_{irrad}–Irradiation temperature (430C - 500C)

FIG. 2.8. Trends in the UTS and % uniform elongation of SS 316 cladding with dpa.

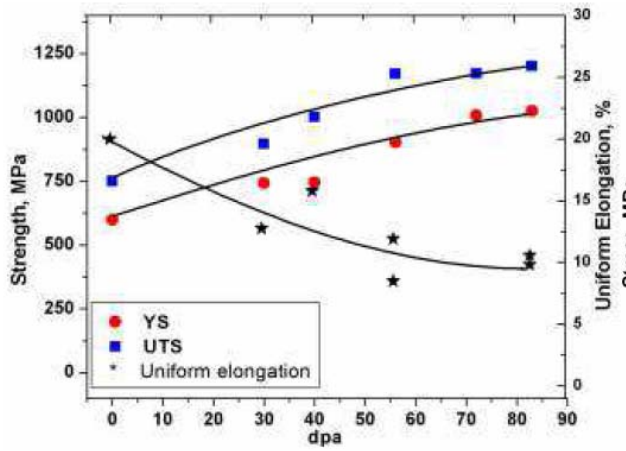

FIG. 2.9. Trends in the room temp. mechanical properties of SS316 wrapper as a function of 'dpa'.

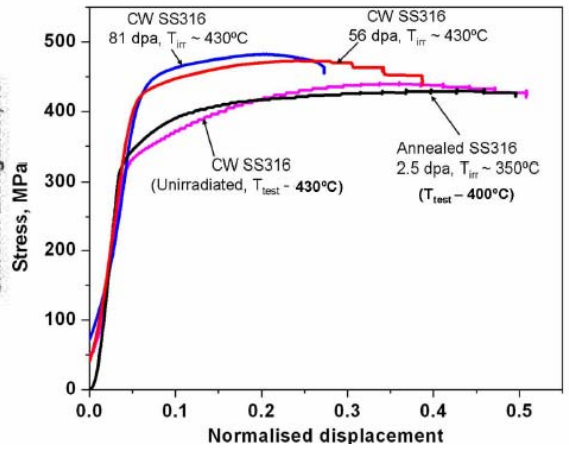

FIG. 2.10. Stress-normalised displacement plots of high temperature shear punch tests on wrapper.

Electron microscopic studies of SS316 cladding and wrapper

Transmission electron microscopy (TEM) studies of hexagonal wrapper showed extensive void formation beyond 40 dpa in addition to precipitation and dislocation loops. Fig. 2.11 shows the TEM micrographs at different dpa superimposed on the swelling curve. The void density showed a progressive increase with displacement damage. The precipitates were identified to be mainly of nickel and silicon enriched M6C type of η phase, whereas radiation induced G phase was also observed at 83 dpa. The precipitates were found to be associated with the voids possibly due to the growth of precipitates by diffusion of solutes along with surplus vacancies. The retention of cold worked structure was unambiguously seen even after 83 dpa which suggests that no recrystallisation has taken place and irradiation hardening is more prominent than the softening effects as indicated in tensile properties [7].

To characterize the fr acture surfaces of the tensile tested specimens, fractography of the irradiated clad specimens was carried out by extracting the fractured region of the sample and subsequent examination in SEM. Three fracture specimens have been extracted from the tensile tested clad tubes corresponding to dpa levels of 13 dpa, 56 dpa and 83 dpa. Examination of the clad sample exposed to 13 dpa showed features similar to that of un-irradiated cladding. Fracture mode was found to be ductile with numerous dimples on the fracture surface. Examination of 56 dpa sample showed mixed mode of fracture with predominantly brittle fracture. Faceted surfaces typical of channel fracture reported in irradiated austenitic stainless steel, were observed [8].

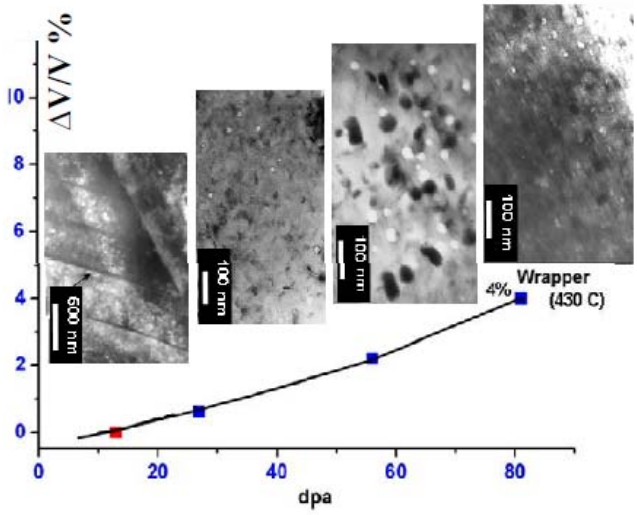

FIG. 2.11. TEM micrographs of SS316 wrapper at various dpa superimposed on swelling curve.

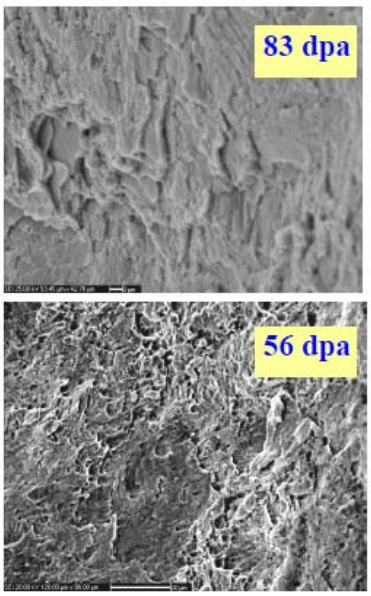

Fig. 2.12. SEM fractographs of irradiated cladding after 56 dpa and 83 dpa.

Fractography of 83 dpa sample shows completely brittle faceted surfaces. No indication of ductile fracture was observed in 83 dpa sample. Fig. 2.12 shows the SEM fractographs of 56 dpa and 83 dpa clad samples. The above observations correlate well with the measured tensile properties of the irradiated clad at different 'dpa' levels.

PIE of FBTR mixed carbide fuel at different burnup levels has indicated excellent performance of the fuel. The burnup limits arising out of various factors such as fuel swelling, porosity exhaustion, metal phase formation, fuel-clad chemical interaction etc. were thoroughly analysed and it was found that fuel performance is not a life limiting factor. The main limiting factors for further enhancing the burn-up were (i) dilation of wrapper and its impact on the fuel handling operations and (ii) loss of cladding mechanical properties. The thermo-mechanical analysis of the fuel subassembly based on the PIE results indicated possibility of a marginal increase in the fuel burn-up beyond 155 $GW \cdot d \cdot t^{-1}$. The burn-up of a one representative subassembly has been increased to 165 $GW \cdot d \cdot t^{-1}$.

3. POST IRRADIATION EXAMINATION OF CONTROL ROD ASSEMBLY OF FBTR

FBTR has six control rod assemblies with sintered boron carbide pellets (90% enriched in ^{10}B isotope) inside SS316 cladding. One of the control rods was discharged after subjecting to a fluence level of 7.0×10^{22} $n \cdot cm^{-2}$ to assess its irradiation behavior and to investigate the cause of excessive load encountered during raising of control rod beyond a particular axial position. It was also required to assess the swelling behaviour of boron carbide (B4C) pellets since volumetric expansion is one of the life limiting factors of the control rod [9]. The control rod is of vented type design having nine boron carbide pellets stacked to a length of 430 mm inside the cladding. It moves axially inside an hexagonal sheath made of SS316 during raising/lowering and the interfaces have stellite coating/tracks. The design fluence limit of FBTR control rod is 1.14×10^{23} $n \cdot cm^{-2}$.

Examinations carried out on the control rod assembly include precise dimensional measurements to investigate the possibility of interference between the control rod and the outer sheath which can result in excessive load, neutron radiography and X-radiography to assess the integrity of the boron carbide pellets and other internals of the control rod, density measurements to assess the swelling behaviour of boron carbide pellets and metallographic examinations to study the cracking behaviour and

microstructural changes in the pellet and the clad. Laser ablation mass spectrometry was done to estimate the depletion of ^{10}B in the pellets.

Dimensional measurements did not indicate any significant changes in the outside diameters of the control rod or the inner diameters of the stellite tracks of outer sheath. Minor misalignments of the order of 1.01 mm and 0.83 mm were observed in the axes of the control rod and the outer sheath. This could have led to the interference between them during raising of power when the shoulder region of the control rod begins to enter the top stellite track of the outer sheath.

Neutron radiography revealed that control rod internals are intact without any blockages which can restrict coolant flow (Fig. 3.1). No gross depletion of ^{10}B was observed. Extensive cracking and fragmentation were observed in the X-radiographs particularly in the bottom pellets which have been exposed to higher neutron fluence. Fig. 3.2 shows the X-radiographs of the boron carbide pellets inside the control rod. X-radiographs did not indicate any significant change in dimensions of the pellets.

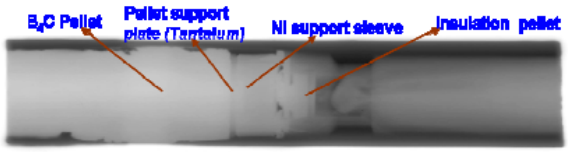

FIG. 3.1. Neutron radiographs of the bottom portion of control rod showing support sleeve, insulation pellet and boron carbide pellet.

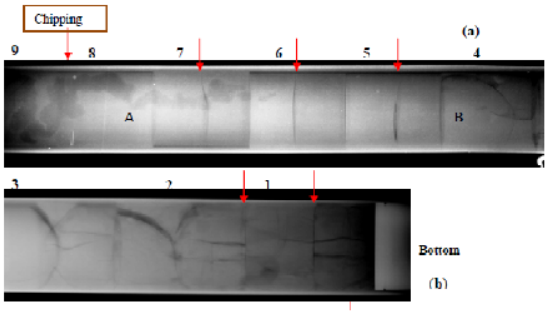

FIG. 3.2. X-radiographs of B4C pellets in the control rod (a) top portion, (b) bottom portion.

The control rod was cut using laser beam on a dismantling bench to retrieve the pellets from the clad. Infiltration of sodium was observed within the fragmented pellets in the bottom region. Extraction of bottom pellets was difficult due to the expansion of the pellet by the presence of frozen sodium within the fragments.

Maximum volumetric swelling of around 2% was estimated from the density measurements of the pellets. Ceramographic examination of three pellets each from the top, middle and bottom regions of the pellet column showed extensive cracking of the bottom pellet. No significant change in the microstructure was observed in the three pellets examined. Metallographic examination of the control rod cladding was carried out to study the interaction of boron carbide pellet and the cladding. The microstructure of the clad cross-section did not indicate any significant interaction between the boron carbide pellet and stainless steel cladding, revealing absence of absorber-clad chemical interaction as observed by optical microscopy.

The isotopic ratio of $^{10}B/^{11}B$ was determined using Laser ablation mass spectrometer. The mass spectrum clearly revealed the presence of ^{7}Li in the irradiated pellets confirming the consumption of ^{10}B. However, ^{10}B depletion in all the pellets was found to be less than 1%.

PIE of control rod assembly has provided valuable information regarding the dimensional changes in the control rod, pellet integrity, swelling behaviour and B10 depletion in B4C pellets. It has been concluded that the excessive load encountered during raising of the control rod could be due to the marginal interference between control rod and outer sheath. Pellet integrity assessment indicated that due to extensive cracking and fragmentation, it may not be possible to reuse most of the pellets. The

PIE has clearly indicated that the boron carbide pellets and the structural materials have not reached life limiting conditions.

4. PIE OF FBTR NICKEL REFLECTOR SUBASSEMBLY

One nickel reflector subassembly was discharged from the 4th ring of FBTR core after attaining a fluence level of 1.09 × 10^{23} n·cm^{-2}. The design fluence limit for nickel subassembly is 1.14 × 10^{23} n·cm^{-2}. Nickel subassembly was subjected to PIE to assess the swelling of the nickel blocks, condition of the collapsible tube inside the nickel subassembly and the radial gap between the nickel blocks and he hexagonal wrapper. It is well known that neutron induced swelling is higher in high purity nickel than that of nickel with impurity content [10]. Nickel blocks used in FBTR reflector subassembly have an impurity content of 0.6%.

PIEs carried out on the nickel subassembly include non destructive examinations such as neutron radiography and gamma autoradiography to examine the internals of the nickel subassembly such as the collapsible tube and the spacing between the hexagonal wrapper and the nickel blocks. Dimensional measurements were done on the hexagonal wrapper and the nickel blocks after dismantling the subassembly and retrieving them from the wrapper. Volume and density of the nickel blocks were measured to estimate the irradiation induced swelling.

Neutron radiography has indicated that the collapsible tube has undergone deformation due to axial expansion of the nickel blocks (Fig. 4.1). Interior of the subassembly was found to be free of sodium and the nickel blocks could be retrieved without any difficulty. Dimensional measurements on the nickel blocks have revealed that the radial gap between the blocks and the hexagonal wrapper has reduced from 3–2 mm. Total axial expansion of the nickel blocks has been measured to be 7 mm. This has been confirmed from gamma autoradiography of the head portion of the subassembly. Density measurements carried out on the nickel blocks have indicated that the maximum volumetric swelling is of the order of 3.6%. This correlates well with the dimensional measurements. Fig. 4.2 shows the density variation in the nickel blocks.

FIG. 4.1. Neutron radiograph of nickel subassembly showing the collapsible tube.

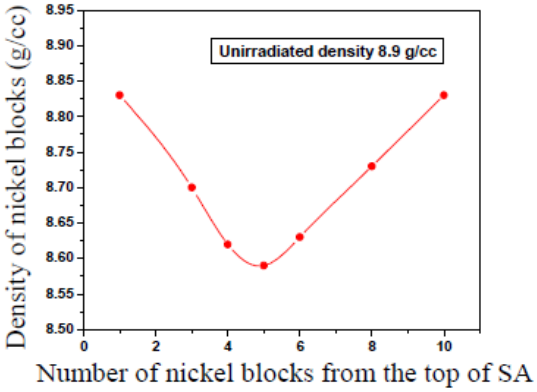

FIG. 4.2. Density variation in the nickel blocks.

PIE of the nickel reflector subassembly has indicated that radial gap is still available between the nickel blocks and the hexagonal wrapper and enough margin is available for accommodating axial expansion of the nickel blocks. The life of other nickel reflector subassemblies in the core can be extended further without any concern regarding the mechanical interaction between the nickel blocks and the wrapper.

5. BEGINNING-OF-LIFE GAP CLOSURE BEHAVIOUR OF EXPERIMENTAL PFBR MOX FUEL PIN

The Protoype Fast Breeder Reactor (PFBR) will use mixed oxide fuel with two different PuO_2 compositions, 21±1% and 28±1% for the two enrichment zones. The fuel pellets are of annular type designed to operate at a peak linear heat rating (LHR) of 450 $W \cdot cm^{-1}$. However, the fabrication tolerances in the fuel pellet dimensions may result in higher fuel-clad-gap resulting in lower gap conductance. To limit the central line temperature within the permissible limits, linear heat rating of fresh fuel will be limited to 400 $W \cdot cm^{-1}$ in the initial phase. Subsequent to the restructuring of the pellet by swelling and cracking and resulting improvement in the gap conductance, LHR will be enhanced to the rated power of 450 $W \cdot cm^{-1}$.

To evaluate the beginning-of-life gap-closure behaviour and to arrive at the optimum duration of preconditioning of fresh fuel, an experimental MOX fuel pin of PFBR fuel composition $(U0.71Pu\ 0.29)O_2$ was irradiated in FBTR for a duration of 13 days in an irradiation capsule at a maximum linear power of 400 $W \cdot cm^{-1}$. This fuel pin has a fissile column length of 240 mm. The fuel pin was extracted from the capsule in the hot cells, sectioned at five axial locations along the length of the fuel column and remote metallography was carried out on these sections.

Fuel-clad radial gap was estimated from the metallographic images at six circumferential locations in the fuel-clad cross-sections. The average radial gap was calculated and compared with that of the unirradiated fuel pin. The typical photomosaic of the fuel pin cross-section at the centre of the fuel column (120 mm from the top of the fuel column) is shown in Fig. 5.1. The photomicrograph shows the presence of a few radial cracks. Polished fuel cross-section was chemically etched for microstructural examination. Fig. 5.2 shows the microstructure having evidence of grain growth in the intermediate zone of the pellet.

PIE has revealed that the fuel-clad gap has reduced considerably from the pre-irradiation radial gap of around 75–110 micrometers to around 13 micrometers throughout the fuel column length after irradiation for 13 days. Cracking of the pellets and relocation of the fuel has resulted in reduction of the fuel-clad gap. The early closure of the fuel-clad gap is a valuable feedback indicative of the optimum preconditioning period required for the fresh fuel before enhancing the LHR to the design value.

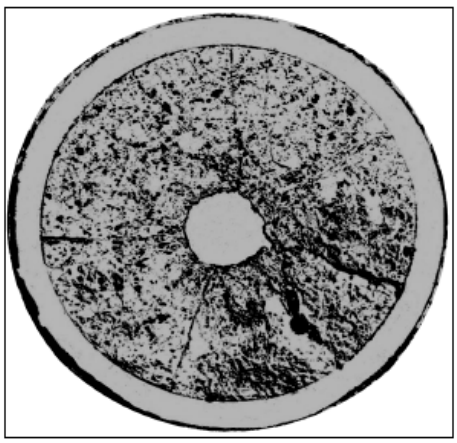

FIG. 5.1. Photomosaic of MOX fuel pin cross-section at the centre of the fuel column.

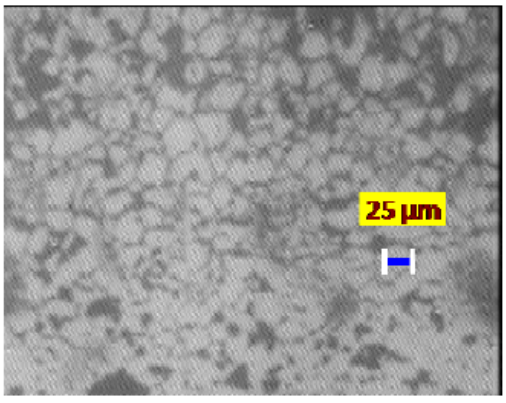

FIG. 5.2. Microstructure of MOX fuel pin.

6. MECHANICAL PROPERTY EVALUATION OF FBTR GRID PLATE MATERIAL

FBTR has been in operation for more than 25 years. As a part of the life extension programme of the FBTR, an assessment of the irradiation induced degradation of FBTR grid plate was undertaken. The performance of the grid plate which supports the core subassemblies is one of the factors considered for extending the life of FBTR. The grid plate of FBTR (SS316) operating at a temperature of about 350°C experiences a cumulative neutron dose of a few dpa over its life time. An accelerated rradiation experiment was performed in FBTR to characterize the mechanical property changes of the SS316 grid plate material subjected to low dose irradiation.

The experimental subassembly used for this test consisted of an irradiation capsule with five compartments in which prefabricated miniature tensile and disc specimens of FBTR grid plate material (SS316) were stacked. The experimental assembly was irradiated in the 4th ring of FBTR for a duration of 58.18 EPFD. The temperature of the irradiation was around 350°C and the accumulated displacement damage ranged from about 1.08 dpa (displacement per atom) to a maximum of 2.57 dpa at the center of the capsule.

The irradiated experimental subassembly was received in hot laboratory (RML) and dismantled using laser cutting to retrieve the irradiated tensile and disc specimens. Remote tensile tests were carried out on the irradiated tensile specimens at temperatures of 25°C, 350°C and 400°C using a universal testing machine installed in the hot cells. As conventional or readily available grips did not exist for ambient/elevated temperature tests of miniaturized tensile specimen (12.7 mm gage length, 3 mm gage width, 1 mm thick), considerable efforts went into development of miniaturized wedge type grips and accessories for carrying out the remote tensile tests.

The stress-strain curves of the irradiated SS316 tested at 350°C are shown in Fig. 5.3. It can be seen that the irradiated SS316 undergoes an increase in YS and UTS with respect to the unirradiated values for all the dpa conditions. Up to 1.08 dpa, this hardening results in negligible changes in uniform elongation (UE). Above 1.08 dpa, the increase in YS is considerably higher than the increase in UTS. The narrowing of the difference between YS and UTS with increase in dpa results in the reduction of uniform elongation to about 20% for the specimen irradiated to 2.57 dpa. The trends in the YS, UTS and % UE of irradiated SS316 tested at 350°C are shown in Fig. 5.4. These results are consistent with the results of irradiated SS316 reported in the literature [11]. The effect of low dose neutron irradiation on the material properties is considered in the design standard of FBR structural materials by limiting the accumulated neutron irradiation to maintain ductility above 10%. A uniform elongation of above 20% at test temperatures of 28°C, 350°C and 400°C of SS316 indicates retention of adequate ductility in SS316 grid plate of FBTR for an accumulated fast neutron dose of 2.57 dpa.

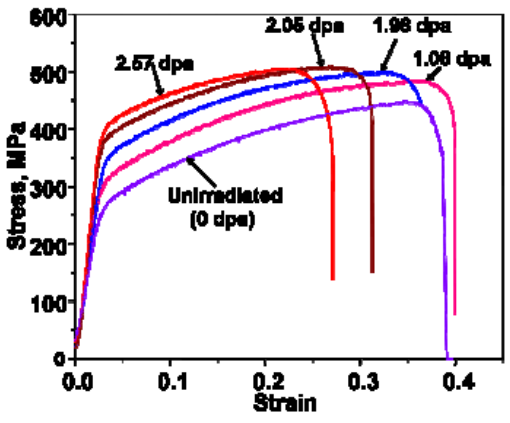

FIG. 5.3. Stress-strain curves of SS316 irradiated to various displacement damages and tested at 350°C.

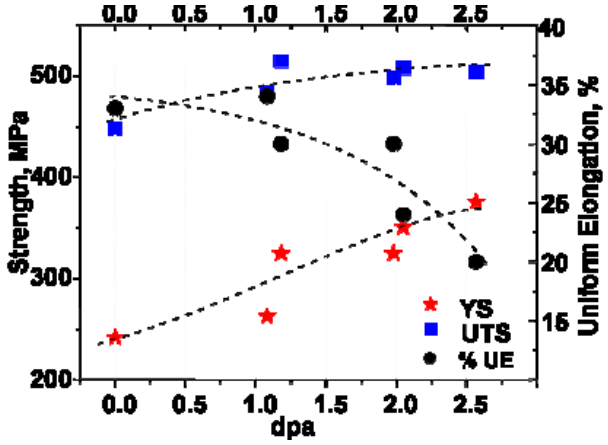

FIG. 5.4. Trends in YS, UTS and % UE of irradiated SS 316 tested at 350°C as a function of dpa.

7. SUMMARY

The stage wise performance assessment of the plutonium rich mixed carbide fuel of the Fast Breeder Test Reactor (FBTR), starting from beginning-of-life performance studies and subsequently at various stages of burn-up has led to a comprehensive understanding of the fuel and structural material irradiation behaviour. Compared to the initial design limit of 50 $GW \cdot d \cdot t^{-1}$, the burn-up reached 165 $GW \cdot d \cdot t^{-1}$ for the plutonium rich mixed carbide fuel. PIE has thus played a crucial role in validating the design and choice of the unique fuel material of FBTR, thereby increasing its in-reactor life. Besides the driver fuel assembly, the performance evaluation of various other core materials like the control rod subassembly and nickel reflector subassembly has provided valuable information on swelling and dimensional changes under fast neutron irradiation. Mechanical property evaluation of grid plate material has provided crucial feedback for the life extension programme of FBTR. PIE inputs from the examination of PFBR MOX fuel will be significant for the economical operation of PFBR.

8. ACKNOWLEDGEMENTS

Authors gratefully acknowledge the guidance and support of Mr. S.C. Chetal, Director, IGCAR during the course of the reported work. The contributions of the colleagues from various groups such as reactor design, reactor operations, physical metallurgy and the chemistry group of IGCAR and Radiometallurgy Division, BARC are also acknowledged.

REFERENCES

[1] RAJ, B., et al., Post Irradiation Examination of mixed (Pu, U)C fuels irradiated in the Fast Breeder Reactor, IAEA Proceedings IAEA-TECDOC-1039 on Influence of High Dose Irradiation on Core Structural and Fuel Materials in Advanced Reactor, Obninsk (1997) 57–68.

[2] KASIVISWANATHAN, K.V., VENKATRAMAN, B., RAJ, B., Neutron radiographic facilities available with KAMINI, Proceedings of 6th World Conference on Neutron Radiography, (Ed. Shigenori Fujine, Hisao Kobayashi and Keiji Kanda, Gordon) Breach Science Publishers, Tokyo (1999) 117.

[3] KASIVISWANATHAN, K.V., MURALIDHARAN, N.G., VIJAYARAGHAVAN, A., JOSEPH, J., VENUGOPAL, V., KASIVISWANATHAN, K.V., Estimation of fission gas release in FBTR fuel pins, Int. Journal of Nuclear Energy Science and Technology. **2** (2006) 352.

[4] MURALIDHARAN, N.G., VENKITESWARAN, C.N., KARTHIK, V., MANOJKUMAR, P.A., SOSAMMA, S., RAO, S.B., VENUGOPAL, V., KASIVISWANATHAN, K.V., Remote metallographic examination of mixed carbide fuel of Fast Breeder Test Reactor at Radio Metallurgy Laboratory, Int. Journal of Nuclear Energy Science and Technology, **1** (2005) 191.

[5] GARNER, F.A., Irradiation performance of cladding and structural steels in liquid metal reactors, in Nuclear Materials, Part 1, Materials Science and Technology - Vol. 10A, (Eds. Frost B.R.T), VCH Publishers (1993) 420.

[6] POROLLO, S.I., KONOBEEV, Yu.V., GARNER, F.A., Swelling and microstructure of austenitic stainless steel ChS-68 CW after high dose neutron irradiation, J. Nucl. Mat. **393** (2009) 61.

[7] VENKITESWARAN, C.N., KARTHIK, V., PARAMESWARAN, P., MURALIDHARAN, N.G., RAJ, V.A., SAROJA, S., VENUGOPAL, V., VIJAYALAKSHMI, M., KASIVISWANATHAN, K.V., RAJ, B., Study of microstructure and property changes in irradiated SS316 wrapper of Fast Breeder Test Reactor, ASTM STP 1513 (2010) 196–209.

[8] HUANG, F.H., The fracture characterization of highly irradiated type 316 stainless steel, International Journal of Fracture **25** (1984) 181–193.

[9] INTERNATIONAL ATOMIC ENERGY AGENCY, Absorber materials, control rods and designs of shutdown systems for advanced liquid metal fast reactors, IAEA-TECDOC—884, IAEA,Vienna (1995).

[10] HOLMES, J.J., Irradiation induced swelling in nickel alloys, Transaction of American Nuclear Society, Vol. 12 (1969) 117.

[11] TAVASSOLI, A.A., PICKER, C., WAREING, J., Data collection on the effect of irradiation on the mechanical properties of austenitic stainless steels and weld metals, Effect of Radiation on Materials, ASTM STP 1270 (1996) 995.